^{18}F-alfatide positron emission tomography may predict anti-angiogenic responses

JIE LIU[1,2], DONGXU WANG[1,2], XUE MENG[2,3], XINDONG SUN[2,3], SHUANGHU YUAN[2,3] and JINMING YU[2,3]

[1]School of Medicine and Life Sciences, University of Jinan-Shandong Academy of Medical Sciences, Jinan, Shandong 250022; [2]Department of Radiation Oncology, Shandong Cancer Hospital Affiliated to Shandong University, Jinan, Shandong 250117; [3]Shandong Academy of Medical Sciences, Jinan, Shandong 250022, P.R. China

Received May 2, 2018; Accepted September 3, 2018

DOI: 10.3892/or.2018.6692

Abstract. As the crucial issue in the development of anti-angiogenic drugs is how to predict which patients will and will not benefit prior to the initiation of therapy, angiogenic ^{18}F-alfatide positron emission computed tomography (PET) was assessed in the present study. Lung adenocarcinoma A549 (high angiogenesis) and prostate PC-3 (low angiogenesis) cell xenografted tumor-bearing mice underwent ^{18}F-alfatide PET at baseline and following treatment with either an anti-angiogenic therapy or vehicle. The evaluation index for the inhibition of tumor growth in the individuals in the treated groups was represented by treatment/control (T/C) ratio (%). Anti-angiogenic responses were denoted by the changes in ^{18}F-alfatide uptake in the same animal. The T/C ratio was lower in high-uptake tumors than in low-uptake tumors (P=0.001). A significant difference in the tumor volumes between the anti-angiogenic therapy group and the control group occurred earlier in the A549 model than in the PC-3 model. ^{18}F-alfatide uptake decreased more for A549 tumors than for PC-3 tumors following anti-angiogenic therapy. In each treatment group, the degree of tumor response to anti-angiogenic therapy was associated well with the tumor uptake prior to treatment (P<0.05). These results indicated that ^{18}F-alfatide PET may be a useful molecular imaging tool for individual selection prior to anti-angiogenic drug therapy.

Introduction

Angiogenesis, the process of new blood vessel formation from the pre-existing vasculature, is recognized as the key for tumor growth and progression (1). Solid tumors cannot grow beyond 1-2 mm in size without a blood supply from the neovasculature (2). In 1971, Folkman (3) first proposed the concept of cancer treatment via the inhibition of new blood vessel formation in tumors. Studies of tumor angiogenesis progressed slowly until the identification of crucial molecules, namely, the vascular endothelial growth factor (VEGF) family and their cognate receptors (4). Even though anti-angiogenic drugs have yielded significant results, extension of progression-free survival and, in certain cases, overall survival times are small (5). The benefits of anti-angiogenic agents are markedly inconsistent among different tumor types (5). The finding of inter- and intra-angiogenic heterogeneity may promote the improvement of the current applications of anti-angiogenic therapy (6). Thus, the vital issue in the development of such drugs is the establishment of early clinical predictors of treatment response in order to predict the patients that may or may not benefit prior to therapy initiation. Understanding angiogenic heterogeneity may help guide treatment strategies.

Integrins, as important mediators in cell-cell and cell-matrix interactions, serve key roles in angiogenesis and tumor metastasis (7). Several integrins, particularly integrin αvβ3, are significantly upregulated in various types of tumor cells and in activated endothelial cells during angiogenesis, but these integrins are not at all, or only slightly, affected in quiescent vessel cells and other normal cells (8). Therefore, imaging of integrin αvβ3 expression is a potential method for evaluating tumor neovascularization. The majority of integrin-targeted imaging tracers function based on the tripeptide Arg-Gly-Asp (RGD) amino acid sequence due to its high affinity and specificity for integrin αvβ3 (9). ^{18}F-alfatide, with the advantages of easy preparation, one-step labeling and fast pharmacokinetics *in vivo*, has been found to be safe (10). Positron emission tomography (PET) was chosen as the imaging strategy due to its high sensitivity to low amounts of tracer and its exquisite specificity (11). Animal experiments have shown that ^{18}F-alfatide PET is an effective tracer for tumor spatial heterogeneity imaging (12), allowing further investigation of the angiogenic heterogeneity among different tumors. In addition, we have performed two pilot clinical studies in which ^{18}F-alfatide PET/CT parameters were found to predict tumor sensitivity to concurrent chemoradiation therapy (CCRT) in patients with gliomas and advanced non-small cell lung cancer (NSCLC) (13,14). Therefore, we hypothesized that ^{18}F-alfatide PET may be able to predict anti-angiogenic responses.

Correspondence to: Dr Shuanghu Yuan or Dr Jinming Yu, Department of Radiation Oncology, Shandong Cancer Hospital Affiliated to Shandong University, 440 Jiyan Road, Jinan, Shandong 250117, P.R. China
E-mail: yuanshuanghu@sina.com
E-mail: sdyujinming@163.com

Key words: ^{18}F-alfatide positron emission tomography, integrin αvβ3, anti-angiogenic therapy, response prediction, heterogeneity

The present animal study aimed to investigate whether ^{18}F-alfatide PET parameters could be used to predict the response to anti-angiogenic therapy in a lung adenocarcinoma A549 xenograft model, which had a high vessel density and high αvβ3 expression, and in a prostate cancer PC-3 xenograft model, which had a low vessel density and low αvβ3 expression.

Materials and methods

Drugs. The agents used in the present study were bevacizumab (Avastin; Roche Diagnostics, Basel, Switzerland), apatinib (Jiangsu Hengrui Medicine Co., Ltd., Jiangsu, China) and cisplatin (Qilu Pharmaceutical, Co., Ltd., Jinan, Shandong, China). Bevacizumab and cisplatin were dissolved in physiological saline. Apatinib was diluted in 0.5% (w/v) carboxymethyl cellulose and 5% (w/v) glucose solution.

Cell culture. Human lung adenocarcinoma A549 (high αvβ3 expression) and human prostatic carcinoma PC-3 (low αvβ3 expression) cell lines were purchased from the Type Culture Collection of the Chinese Academy of Sciences (Shanghai, China). These two cell lines were grown at 37˚C in RPMI-1640 medium (Invitrogen; Thermo Fisher Scientific, Inc., Waltham, MA, USA) supplemented with 10% fetal bovine serum and 1% penicillin streptomycin antibiotic mixture (Invitrogen; Thermo Fisher Scientific, Inc.) in a humidified incubator (Heraeus Germany GmbH & Co. KG, Hanau, Germany) with 5% CO_2. Cells were grown as a monolayer and were split or harvested when they reached 80-90% confluence to maintain exponential growth.

Animal models. A total of $2x10^6$ A549 cells or $5x10^6$ PC-3 cells were injected subcutaneously near the right shoulders of female BALB/c nude mice (n=110; age, 6-8 weeks; weight, 18-20 g) purchased from the Beijing Hua Fukang pathogen-free animal breeding facility [approval no. SCXK (Jing) 2009-0008]. A total of $2x10^6$ A549 cells were injected into the right hind leg for radiotherapy. The tumor size and mouse body weight were measured every 2 days, and the tumor volume was calculated with the following formula: Tumor volume = (length x width^2)/2. The index for evaluating the inhibition in individuals in the treated groups was the relative tumor growth ratio, which was calculated according to the following equation: Treatment/control (T/C) (%) = increase in tumor volume in treated individuals/mean increase in tumor volume in the control group x 100 (15). The animal rooms provided a constant temperature of 26˚C, a relative humidity of 50-60% and daylight plus a 12/12-h light/dark cycle. The mice were fed a laboratory animal diet and sterile water *ad libitum*. The maximum tumor volume was ~1,800 mm^3 and multiple tumors were nt observed in any individual animal. A tumor size >20 mm (2.0 cm) in any direction or weight loss exceeding 10% of the original weight were considered humane endpoints.

Experimental design and treatment protocol. A total of 20 size-matched, xenografted tumor-bearing mice (A549, n=10; PC-3, n=10), with a mean tumor volume of 100 mm^3 1 day prior to the PET imaging, were used to compare the tumor uptake of ^{18}F-alfatide between two tumor types and to analyze the angiogenic heterogeneity. The heterogeneity was represented by the coefficient of variation (CV) of ^{18}F-alfatide, calculated by dividing the standard deviation by the mean value.

In an efficacy prediction test, the groups (n=90, 6-8/group) were sized-matched with tumor volumes of 100-200 mm^3 1 day prior to the baseline PET imaging. For anti-angiogenic therapy, A549 and PC-3 xenografted tumor-bearing mice were injected with bevacizumab intraperitoneally or administered apatinib by oral gavage on day 0 after the baseline imaging. Bevacizumab, at a dose of 20 mg/kg body weight in 200 μl saline, or vehicle of 200 μl physiological saline, was administered every 4 days over 2 weeks (four injections). Apatinib, at a dose of 100 mg/kg body weight in 200-μl suspensions, or the vehicle of 200 μl 0.5% (w/v) carboxymethyl cellulose and 5% (w/v) glucose solution, was administered once daily for 2 weeks.

To balance the effects of the two drugs in the combined treatment, preliminary experiments (n=3) were performed to determine whether cisplatin, at a dose of 5 mg/kg body weight (injected intraperitoneally every 3 days for five injections), and radiotherapy of 5 Gy at a time (once a week, two times), could produce similar effects to those of the treatment protocol of bevacizumab over 2 weeks by comparing the tumor volumes between the experimental and control groups (data not shown). In the combined therapy, mice bearing A549 xenografts received chemotherapy or radiotherapy 2 h after bevacizumab in order to obtain a better curative effect during vascular normalization (16). For the radiation treatment, the mice were anesthetized, the tumor-bearing leg was positioned in the radiation field and a lead cover protected the rest of the body. Irradiation was performed with 6 MeV of X-rays using a linear accelerator (X-RAD 225; Varian Medical Systems, Inc., Palo Alto, CA, USA). The dose was administered at the measured depth. The schedule of laboratory assignments is shown in Fig. 1.

Micro-PET imaging protocol. ^{18}F-alfatide micro-PET scans were performed for all 20 tumor-bearing mice when the tumor volume of each mouse reached ~100 mm^3 for the heterogeneity analysis, at 0 and 15 days for anti-angiogenic treatment, and at 0 and 7 days for the combined therapy following the initiation of treatment. A simple lyophilized kit for labeling the PRGD2 peptide was purchased from the Jiangsu Atomic Energy Laboratory (Jiangsu, China), and the synthesis process was performed according to a previously published method (17). The radiochemical purity of the ^{18}F-alfatide exceeded 95%, and its specific radioactivity exceeded 37 GBq (1,000 mCi)/μmol. All the micro-PET images were obtained with an Inveon PET scanner (Siemens Preclinical Solutions, LLC, Knoxville, TN, USA) using ^{18}F-alfatide. With the assistance of the positioning laser from the Inveon system, each tumor-bearing mouse was placed with its tumor located in the center of the field of view to achieve the highest imaging sensitivity.

^{18}F-alfatide PET scans were performed 1 h after tail-vein injection of ^{18}F-alfatide (2.4-3.5 MBq), under isoflurane anesthesia with 1.5% isoflurane in 100% oxygen at a flow rate of 1.5 l/min. Prior to the ^{18}F-alfatide PET scanning, the mice were prohibited from drinking water for at least 4 h. The PET images were reconstructed and analyzed by the OSEM-3D IAM software program (IS_v1.4.3 SP1; Siemens Preclinical Solutions, LLC).

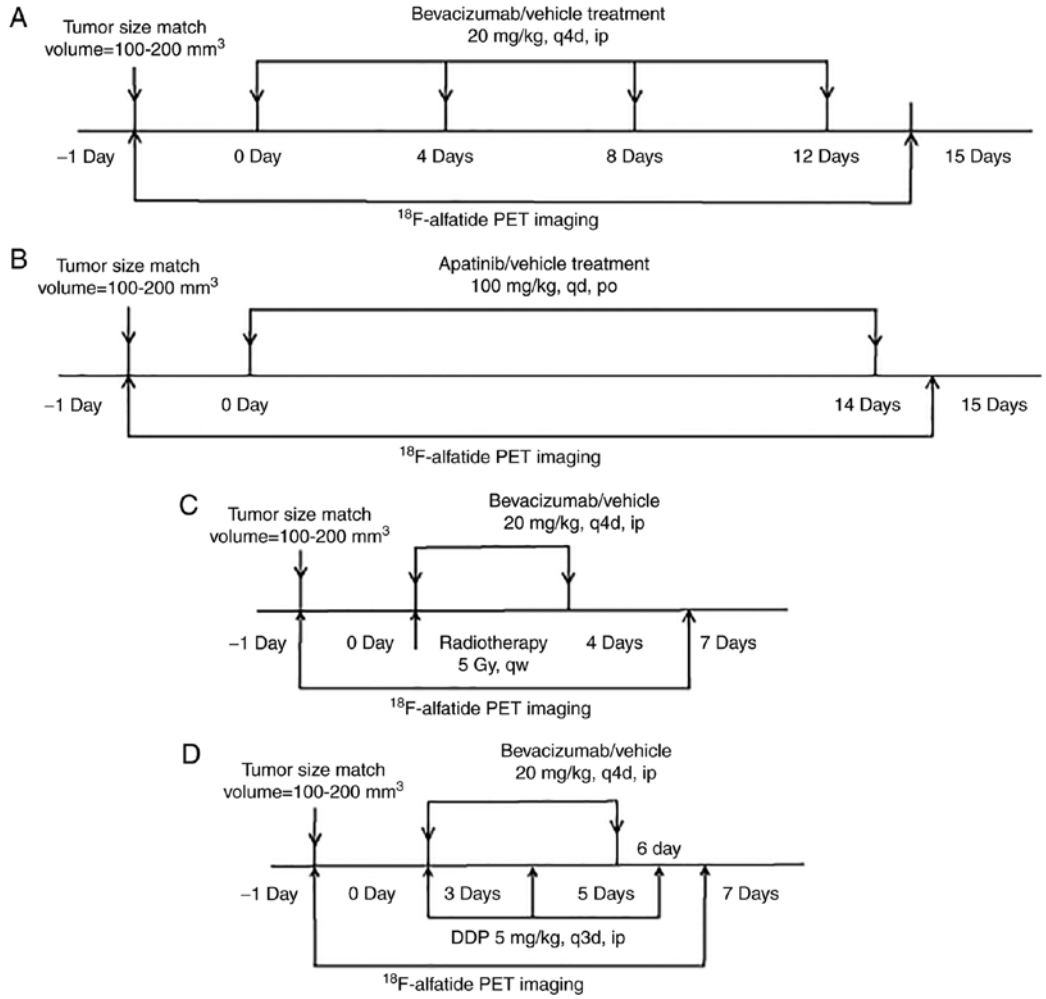

Figure 1. Treatment protocols for (A) bevacizumab, (B) apatinib, (C) bevacizumab combined with radiotherapy and (D) bevacizumab combined with DDP, and the imaging protocol are shown. Tumor size was calculated on the basis of caliper measurements according the formula: (length x width^2)/2. DDP, cisplatin; q4d, every four days; qd, once a day; qw, once a week; ip, intraperitoneal injection; po, oral administration; PET, positron emission tomography.

Image analysis. Two experienced nuclear medicine physicians examined all the images using a double-blinded approach and aimed to reach a consensus. If no consensus was reached, the third chief physician decided the treatment response. Regions of interest (ROIs) were drawn over the tumor using vendor software (IS_v1.4.3 SP1; Siemens Healthineers, Erlangen, Germany) on decay-corrected, whole-body transverse images with a threshold of 40%, and a set of data that included the ROI_{max} and the mean was obtained. The standardized uptake value (SUV) of each tumor was calculated as the maximal or mean trace uptake of the ROIs according to the following formula: [measured activity concentration (Bq/ml) x body weight (g)]/injected activity (Bq). A circular region of 5x5 mm, which was manually contoured in the liver, a relatively large and less active organ, on each transverse PET image was defined as the non-target reference. The tumor-to-normal tissue (T/N) ratio was calculated by taking the ratio of the tumor SUV_{max} to the liver SUV_{max} (18).

Three-dimensional ROIs were drawn using the TrueD tool kit (Siemens Preclinical Solutions, LLC), which involved several imperative manual adjustments. The SUV_{mean} and SUV_{max} were acquired by calculating the average of the SUV_{mean} and the SUV_{max} of the planar ROIs drawn on three discontinuous transaxial PET slices, respectively (6). The CV of each group was calculated by the following formula: Standard deviation (SD)/the mean value of the SUV_{mean}.

Statistical analysis. All data were analyzed using GraphPad Prism 7.0 (GraphPad Software, Inc., La Jolla, CA, USA) and are presented as the mean ± SD. The significance of statistical differences between the two groups was determined by Student's t-tests. One-way analysis of variance and Bonferroni's post hoc test were required for multiple comparisons. Within each group, linear regression analysis was used to evaluate the associations. $P<0.05$ was considered to indicate a statistically significant difference.

Results

Tumor uptake of ^{18}F-alfatide and angiogenesis heterogeneity between the A549 and PC-3 models. As illustrated in Fig. 2, the SUV_{mean} and T/N ratios of ^{18}F-alfatide in the A549 models were significantly higher than those in the PC-3 models (SUV_{mean}, 0.64±0.07 and 0.25±0.02, respectively; $P<0.00001$; T/N, 2.76±0.62 and 0.82±0.11, respectively; $P<0.00001$). The variation coefficients of the 10 tumors in the A549 and PC-3

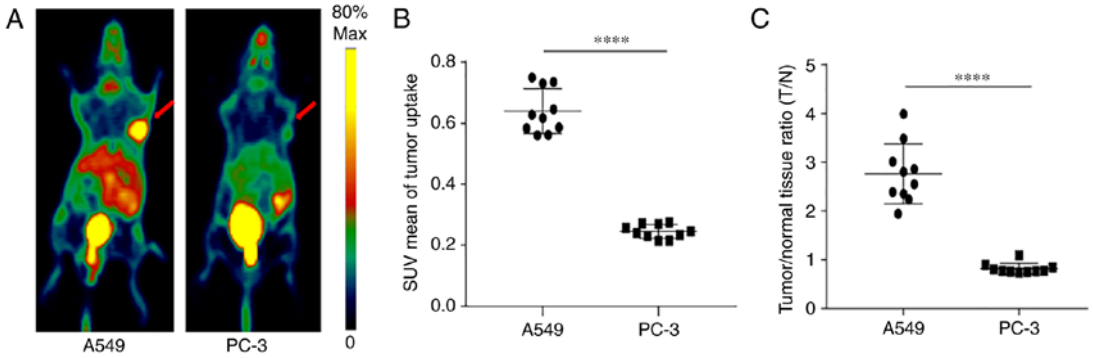

Figure 2. (A) Imaging of xenografted tumor-bearing mice and (B) comparison of the SUV_{mean} and (C) the T/N ratios of ^{18}F-alfatide uptake in the A549 (n=10) and PC-3 (n=10) xenograft tumor-bearing models. The SUV_{mean} and T/N ratios were calculated via quantification of the PET imaging. The tumor is indicated by the red arrow. ****P<0.00001. PET, positron emission tomography; SUV_{mean}, mean standardized uptake value; T/N, tumor-to-normal tissue.

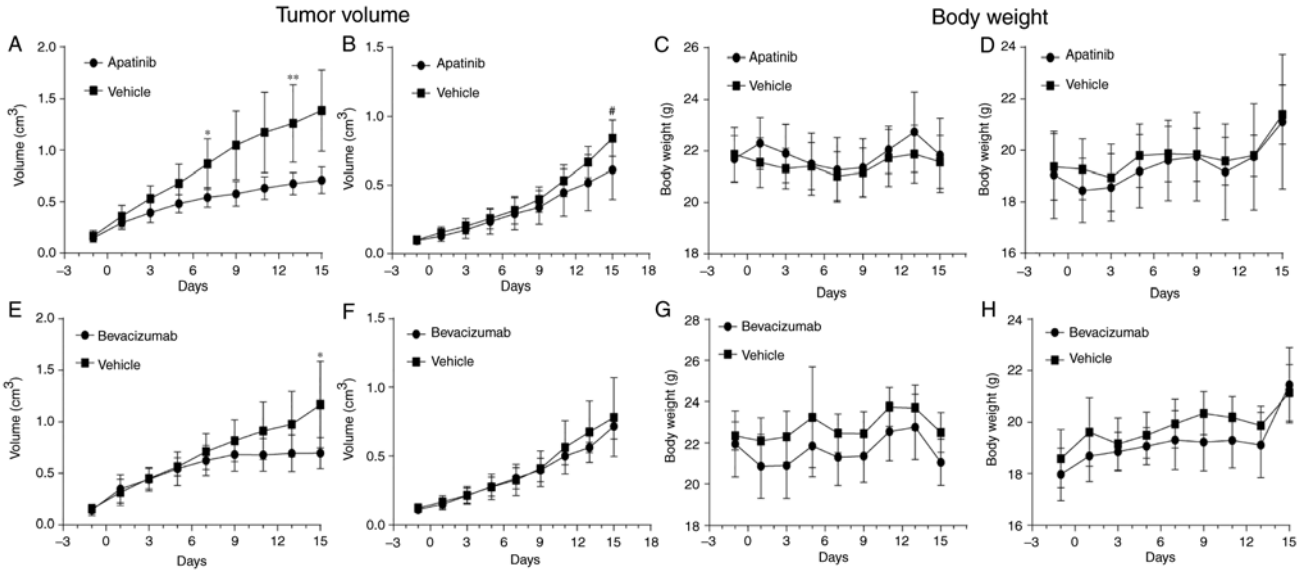

Figure 3. Tumor growth curves and body weight changes for the vehicle- (n=6-8) and apatinib- or bevacizumab-treated (n=6-8) groups in the xenografted A549 lung adenocarcinoma and PC-3 prostate cancer models. (A and B) Tumor growth and (C and D) body weight in apatinib- or vehicle-treated A549 and PC-3 xenografted models; (E and F) tumor growth and (G and H) body weight in the bevacizumab- or vehicle-treated A549 and PC-3 xenografted models. Tumor size was calculated on the basis of caliper measurements according to the formula (length x width^2)/2. Body weight was measured by scales. **P<0.001, *P<0.01 and $^{\#}$P<0.05 vs. vehicle-treated group.

models were 11.44 and 9.21%, respectively, for the SUVmean, and 22.28 and 13.15%, respectively, for the T/N ratios, indicating that there was inter- and intra-angiogenic heterogeneity among the A549 and PC-3 xenografted tumors.

Comparison of tumor responses in the two animal models following anti-angiogenic treatment. The ratio of the tumor growth (T/C) following treatment with the anti-angiogenic drugs was lower in the A549 xenografted tumors compared with that in the PC-3 tumors (apatinib, 47±11.46 and 69±26.74%, respectively, P=0.052; bevacizumab, 57.80±13.82 and 90.27±13.09%, respectively, P=0.001). With regard to tumor responses (Fig. 3), Fig. 3A, B, E and F compares the angiogenic responses of the A549 and PC-3 groups by analyzing the tumor growth curves for the vehicle and the same anti-angiogenic drug. Among the A549 groups receiving anti-angiogenic therapy, there was a significant decrease in tumor volume beginning at day 7 in the apatinib-treated models (P<0.01) and at day 15 in the bevacizumab-treated models (P<0.01) compared with that in the vehicle-treated controls. This response occurred earlier than that in the PC-3 groups, in which the significant difference in tumor volume occurred at day 15 (P<0.05) in the apatinib-treated models, while no significant difference was observed in the bevacizumab-treated models. The difference between the tumor volumes in the apatinib- and vehicle-treated models was greater (P<0.001 at day 13) in the A549 group than in the PC-3 group. As shown in Fig. 3C, D, G and H, neither apatinib nor bevacizumab had toxic effects on the mice, indicated by the absence of significant weight loss compared with that in the control groups.

In Fig. 4, the responses to the same anti-angiogenic drugs were compared between the A549 and PC-3 groups by analyzing the SUV_{mean} of the tumors prior to and following treatment. In the A549 lung adenocarcinomas treated by apatinib, the SUV_{means} decreased significantly (P<0.01), and a

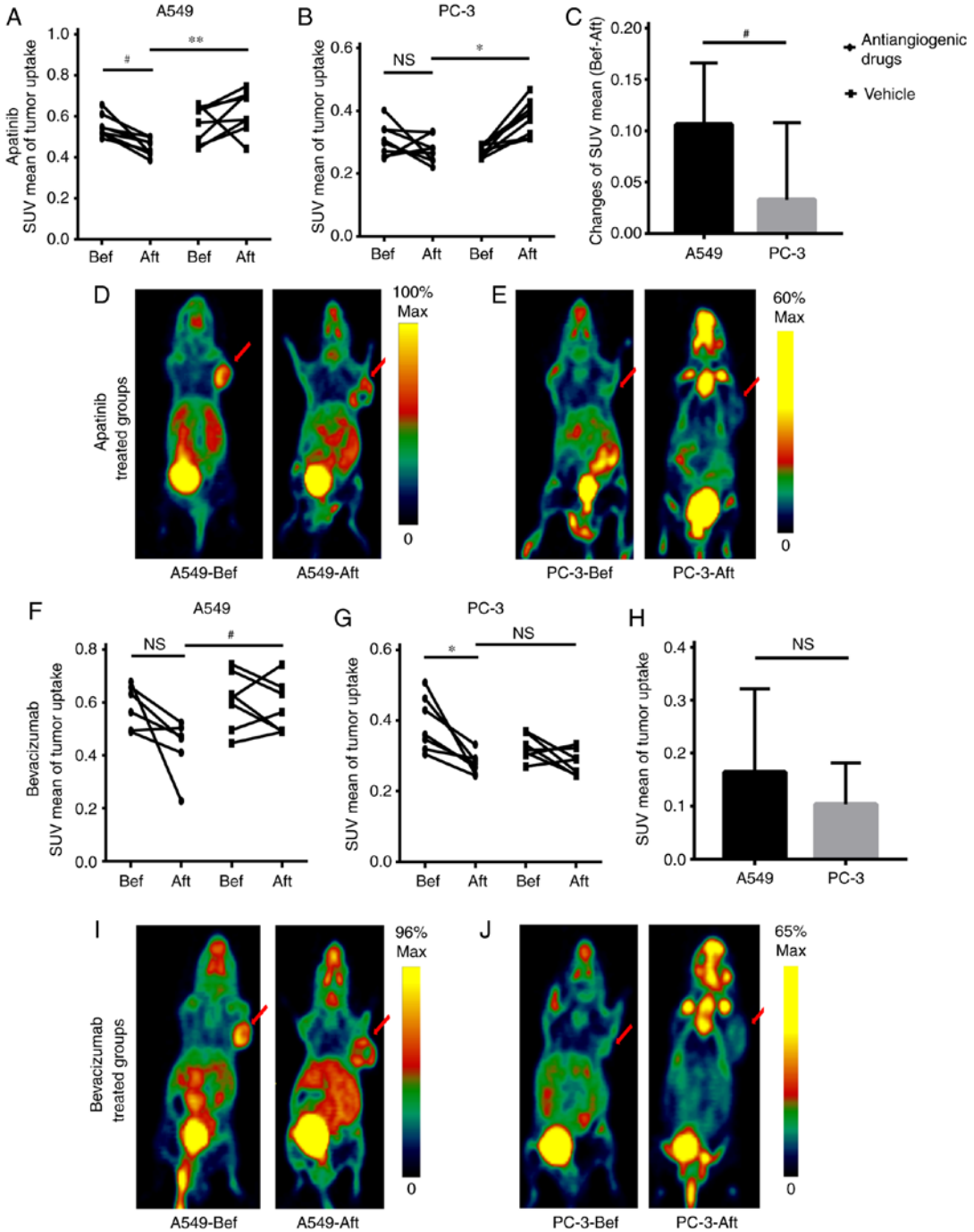

Figure 4. Effect of vehicle and (A and B) 100 mg/kg apatinib and the treatment responses to (C) apatinib in the xenografted A549 lung adenocarcinoma and PC-3 prostate cancer models. (D and E) PET images for apatinib are shown. (F and G) Effect of vehicle and 20 mg/kg bevacizumab, and (H) the treatment responses to bevacizumab in the xenografted A549 lung adenocarcinoma and PC-3 prostate cancer models, and (I and J) PET imaging for bevacizumab are also shown. The effects of antiangiogenic drugs were based on changes in ^{18}F-alfatide uptake (SUV_{mean}) and the treatment responses were in terms of the reduction in ^{18}F-alfatide uptake (SUV_{mean}). PET images are for tumor-bearing mice prior to and following treatment with the anti-angiogenic drugs. The tumor is indicated by the red arrow. **P<0.001, significantly different from the vehicle-treated group following treatment. *P<0.01, significantly different from the vehicle-treated group following treatment in (B) or a significant decrease in ^{18}F-alfatide uptake from the initiation of treatment in (A, F and G). $^{\#}$P<0.05: Significantly different from the vehicle-treated group following treatment in (C) and significantly different responses between A549 and PC-3. ns, P>0.05, not significantly different from the vehicle-treated group, no significant decrease from the initiation of treatment or no significant different responses between A549 and PC-3. SUV_{mean}, mean standardized uptake value.

significant difference between the anti-angiogenic drug- and vehicle-treated models (P<0.001) was observed following treatment. In the PC-3 prostate tumors, only apatinib caused a significant difference in the SUV_{mean} between the treatment and control models (P<0.01) following treatment. Bevacizumab caused a slight decrease in the SUV_{mean} in the treatment group (P=0.06) and a significant difference between the treatment models and control models (P<0.05). However, bevacizumab only caused a significant decrease of SUV_{mean} in the treatment group (P<0.01).

Fig. 4C and H compares the changes in the SUV_{mean} of ^{18}F-alfatide following anti-angiogenic therapy in the two

Table I. Inhibition of tumor growth by apatinib and bevacizumab.

Antiangiogenic drugs	SUV_{mean} prior to treatment	Ratio of individuals <T/C (%)						P-value
		<90%	<80%	<70%	<60%	<50%	<40%	
Apatinib	>0.47			100	87.50	62.5	37.5	0.052
	<0.47			62.5	37.5	12.5	12.5	
Bevacizumab	>0.52	100	85.71	71.43				0.006
	<0.52	50	16.67	0				

Apatinib and bevacizumab groups contained A549 and PC-3 xenografted tumors. T/C (%) = increase in tumor volumes of treated individuals/mean increase in tumor volumes of control groups x100. n=6-8/group. The ratio of individuals <T/C = <T/C individuals/all individual in the groups. The ratios of individuals less than the T/C, except for the data in the table, were similar in the two different uptake groups. P-values are shown for the comparison of the T/C values in the different two groups from the cut-off points. SUV_{mean}, mean standardized uptake value.

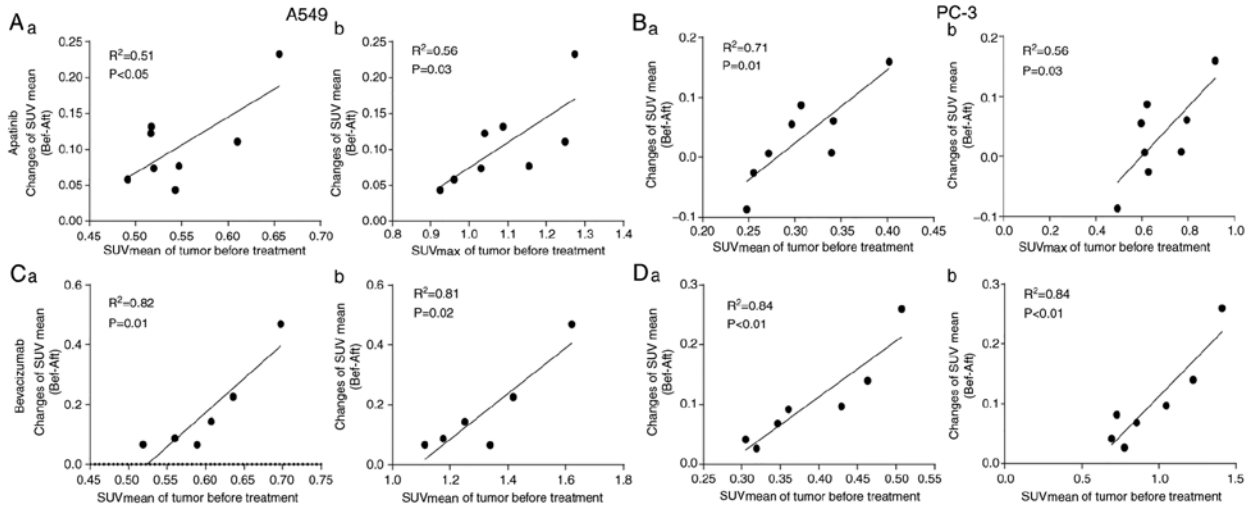

Figure 5. Linear association between the SUV_{mean} changes following (Aa and b; and Ba and b) apatinib and (Ca and b; and Da and b) bevacizumab therapy and the tumor uptake, (Aa, Ba, Ca and Da) SUVmean and (Ab, Bb, Cb and Db) SUV_{max}, prior to treatment in the xenografted (Aa and b, and Ca and b) A549 lung adenocarcinoma and (Ba and b; and Da and b) PC-3 prostate cancer models. The SUV_{mean} changes in ^{18}F-alfatide were calculated by deducting the SUV_{mean} of ^{18}F-alfatide uptake following treatment from its original value on day 0 (prior to treatment) in the same animal. The SUV_{mean} changes were used as an indicator of the tumor responses to anti-angiogenic therapy. SUV_{mean}, mean standardized uptake value; SUV_{max}, maximum SUV.

xenografted tumor-bearing animal models. The degree of tumor response to apatinib or bevacizumab therapy, assessed by the tumor uptake changes of ^{18}F-alfatide (19), was higher in A549 lung adenocarcinomas than in PC-3 prostate tumors. Only SUV_{mean} changes in the tumors following apatinib treatment exhibited a significant difference between the A549 and PC-3 groups (P<0.05). Fig. 4D, E, I and J show the differences in tumor uptake intuitively.

Association between tumor response and tumor uptake prior to treatment with anti-angiogenic therapy. The median of the SUV_{mean} prior to treatment in the apatinib and bevacizumab groups (A549 and PC-3 were included in both groups) was 0.47 and 0.52, respectively. As shown in Table I, the ratios of the individuals whose tumor growth ratio was less than the T/C were greater in the higher SUV_{mean} groups than in the lower SUV_{mean} groups. Fig. 5 shows plots of the SUV_{mean} changes (i.e., the therapeutic effect) following anti-angiogenic therapy against the SUV_{mean} and SUV_{max} in the A549 and PC-3 models at the time of diagnosis. The SUV_{mean} changes were calculated by deducting the SUV_{mean} of ^{18}F-alfatide on day 15 from the SUV_{mean} on day 0 for the same animal. There was a significant positive linear association between SUV_{mean} changes and the tumor uptake prior to treatment in the apatinib-treatment groups (R^2=0.51, P<0.05 for SUV_{mean} prior to treatment and R^2=0.56, P=0.03 for SUV_{max} in the A549 models; R^2=0.71, P=0.01 for SUV_{mean} and R^2=0.56, P=0.03 for SUV_{max} in the PC-3 models). With bevacizumab treatment, there was a higher positive linear association between SUV_{mean} changes and the tumor uptake prior to treatment (R^2=0.82, P=0.01 for SUV_{mean} and R^2=0.81, P=0.02 for SUV_{max} in the A549 models; R^2=0.84, P<0.01 for SUV_{mean} and R^2=0.84, P<0.01 for SUV_{max} in the PC-3 models).

Association between tumor response and tumor uptake prior to treatment with anti-angiogenic therapy combined with chemotherapy or radiotherapy. As shown in Fig. 6A and F, there was a significant decrease in tumor volume in the combined

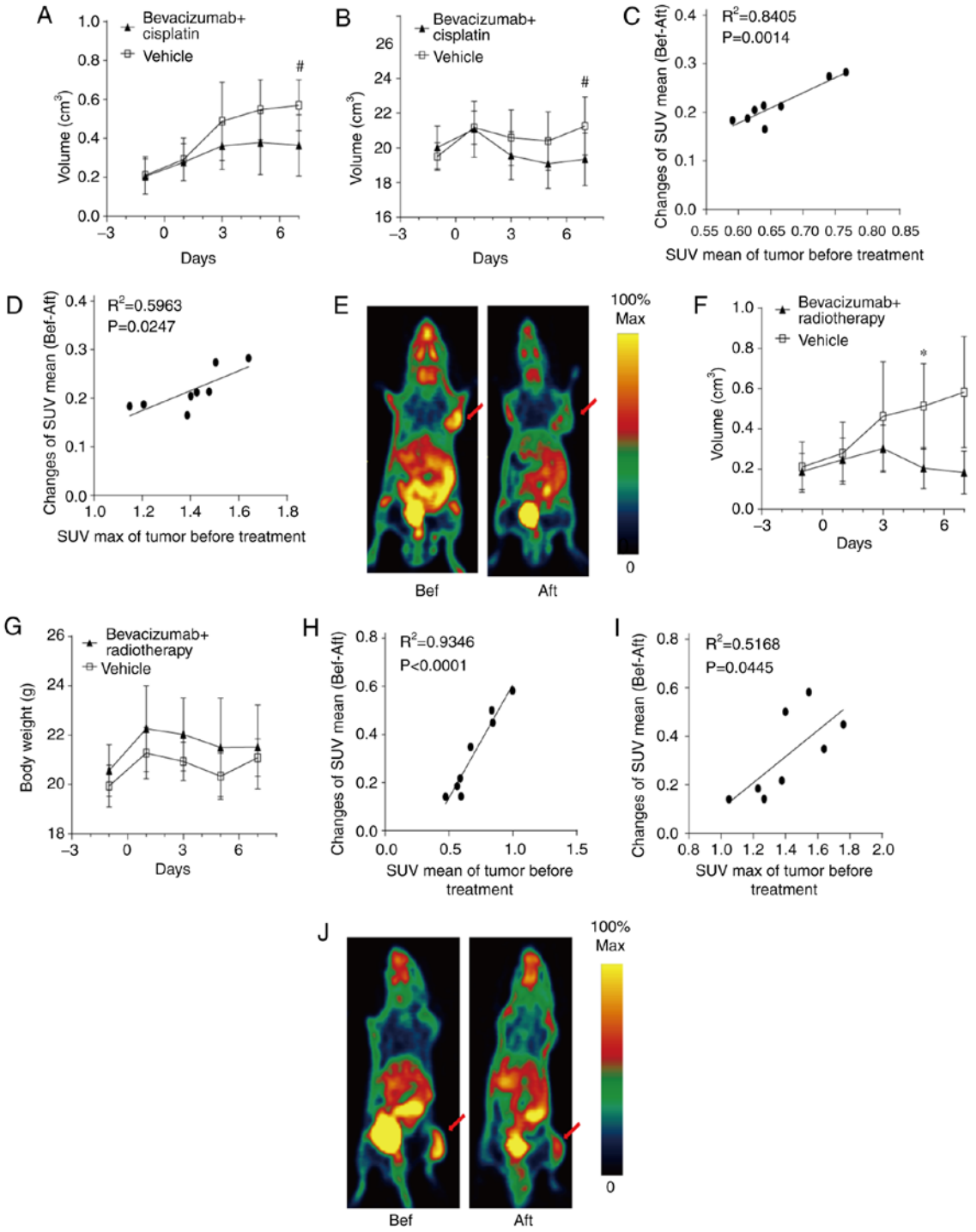

Figure 6. (A) Tumor growth curves, (B) body weight changes, linear associations between the SUV_{mean} changes following treatment with (C) SUV_{mean} and (D) SUV_{max} prior to treatment, and (E) PET imaging for vehicle-(n=8) and bevacizumab combined with cisplatin-(5 mg/kg) in the xenografted A549 lung adenocarcinoma model. (F) Tumor growth curves, (G) body weight changes, linear associations between the SUV_{mean} changes following treatment with (H) SUV_{mean} and (I) SUV_{max} prior to treatment, and (J) PET imaging for vehicle-(n=8) and bevacizumab combined with radiotherapy (5Gy)-treated groups in the xenografted A549 lung adenocarcinoma model. PET imaging of tumor-bearing mice was performed prior to and following treatment with the anti-angiogenic drugs. Tumor volume was determined by caliper measurements. Body weight was measured using scales once every 2 days. The red arrow indicates the tumor. *P<0.01 and $^{\#}$P<0.05, significantly different from the vehicle-treated group. SUV_{mean}, mean standardized uptake value; SUV_{max}, maximum SUV; Bev, bevacizumab.

bevacizumab and cisplatin-treated models compared with that in the vehicle-treated models beginning at day 7 (P<0.05), and the same effect was found with bevacizumab combined with radiotherapy at day 5 (P<0.01). In Fig. 6B and G, bevacizumab combined with cisplatin treatment is shown to have a toxic effect on the mice, as shown by the significant weight loss on the 7th day (P<0.05), and bevacizumab combined with radiotherapy did not have this effect. Fig. 6C, D, H and I shows the linear association between the SUV_{mean} changes following treatment with bevacizumab combined with either cisplatin or

radiotherapy and the uptake of ^{18}F-alfatide by the tumor prior to treatment in the A549 models. There was a significant positive linear association between the SUV_{mean} changes and the SUV_{mean} prior to treatment in the combined bevacizumab and cisplatin-treated models (R^2=0.84, P<0.01) and a moderate linear association between the SUV_{mean} changes and other parameters prior to treatment (R^2=0.60, P=0.02 for SUV_{max}). In mice treated with bevacizumab combined with radiotherapy, the SUV_{mean} changes were associated with the SUV_{mean} prior to treatment (R^2=0.93, P<0.0001) and with the SUV_{max} (R^2=0.52, P=0.04) prior to treatment.

Discussion

In the present study, it was found that the anti-angiogenic treatment response of tumors with high uptake of RGD tracers was better than that of the low-uptake tumors. This result was consistent with the results of the study by Ji *et al* (19), in which the degree of tumor response to linifanib therapy was associated with αvβ3 expression levels prior to treatment. In clinical studies, Iagaru *et al* (20) first found that decreases of >50% in SUV_{max} and angiogenic volumes, assessed by fluorine 18 2-fluoropropionyl-labeled PEGylated dimeric arginine-glycine-aspartic acid peptide (^{18}F-FPPRGD$_2$) uptake, at 1 week after bevacizumab administration predicted good outcomes, while decreases of <15% predicted poor prognoses in patients with glioblastoma multiforme. Subsequently, it was further confirmed that changes in ^{18}F-FPPRGD$_2$ uptake as early as 1 week after bevacizumab administration may be able to predict the outcome of treatment in patients with cervical and ovarian cancer (21). However, all these results were completely contrary to the results of a previous study (14), which demonstrated that tumor uptake in ^{18}F-alfatide PET/CT was higher in non-responders than in responders following CCRT. In the present study, the correlation between tumor uptake prior to treatment and the degree of treatment response in the bevacizumab groups was higher than that in the apatinib groups. The correlation decreased to a moderate level in the bevacizumab combined with chemoradiotherapy group, but remained high in the bevacizumab combined with radiotherapy group. The abnormal structure of neovascularization and the different mechanisms of action of different drugs may be the reason for the opposing conclusions.

Tumor vessels are dilated, tortuous and heterogeneous in their spatial distributions, and are characterized by large inter-endothelial junctions, an increased number of fenestrations and a lack of a normal basement membrane, which makes flow resistance and the hydrostatic and oncotic pressures almost equal between the intravascular and extravascular spaces (22,23). Poor blood flow and elevated interstitial fluid pressure hinder the delivery of therapeutic drugs and oxygen to tumor tissues. Bevacizumab, a recombinant humanized monoclonal antibody that blocks human VEGF from binding to its receptors, could interfere with the ability of a tumor to recruit new blood vessels by binding soluble VEGF in the blood and has no direct effect on the growth of tumor cells *in vitro* (24). As a result, the anti-angiogenic efficiency of bevacizumab may be less affected by vascular structure and function. However, the abnormal microenvironment in tumors could hinder the efficacy of chemotherapeutic drugs, which must pass through the vascular wall to directly act on tumor cells (25). The same is true with radiotherapy in terms of blocking oxygen. It is presumed that it is more difficult for chemotherapeutic drugs and oxygen to reach a tumor with increased immature tumor neovascularization. This may be the reason why tumor uptake in ^{18}F-alfatide PET/CT prior to treatment was higher in non-responders than in responders (P<0.01) (13,14). The negative association between tumor uptake of ^{18}F-alfatide prior to treatment and the degree of the chemoradiotherapy response may reduce the treatment-response association of bevacizumab to a moderate one in the bevacizumab combined with chemotherapy group. In the bevacizumab combined with radiotherapy group, the tumor volumes following therapy were so small that the tumor uptake was very low. Therefore, the SUV_{mean} changes in a tumor mainly depend on the SUV_{mean} prior to treatment. This may have led to the high association between the SUV_{mean} prior to treatment and the response to bevacizumab combined with radiotherapy. Apatinib, an inhibitor of VEGFR-2 tyrosine kinase that targets the intracellular ATP-binding site of the receptor, would also be affected, in that it could inhibit tumor cell growth and tumor angiogenesis during *in vitro* experiments (15). The partial effect of apatinib on antitumor cells may also be influenced by the abnormal neovascular structure. The different mechanisms of action may be the reason for the different degrees of association between the uptake of RGD-based tracers by tumors and the effects of anti-angiogenic therapies.

From the present study, intertumoral angiogenic heterogeneity was found between A549 lung adenocarcinoma and PC-3 prostate cancer, which was indicated by higher levels of tracer uptake in A549 tumors than in PC-3 xenografted tumors. Intratumor angiogenic heterogeneity (CV) also existed among the groups and was higher in the A549 group than in the PC-3 group. RGD-based tracer targeting of αvβ3 has already been used in the diagnosis of malignant tumors (10,26,27) and in predicting the efficacy of CCRT in NSCLC (13,14). Low ^{68}Ga-RGD$_2$ uptake and poor αvβ3 expression in SCLC may have led to the conclusion that αvβ3-targeted therapy is not adequate for the majority of SCLC patients. Clinical research of cilengitide (a type of RGD peptide targeted to αvβ3) was supported in NSCLC, and the treated tumors were characterized by high angiogenesis. However, the relatively conspicuous intratumor angiogenic heterogeneity of NSCLC made the therapeutic response to cilengitide susceptible to variations between individuals (6,20). Therefore, such inter- and intratumoral angiogenic heterogeneity highlights the importance of patient selection prior to αvβ3-targeted or anti-angiogenic therapy. Kang *et al* (6) found that the apparent intratumoral angiogenic heterogeneity in NSCLC and SCLC primary lesions was similar (CV: 36.2 vs. 36.3%), although the SUVs of ^{68}Ga-RGD$_2$ in NSCLC primary lesions were significantly higher than those in SCLC (P<0.0001) (6). From the present study, it was found that the CV of the A549 tumor group (high angiogenesis) was greater than that of the PC-3 group (low angiogenesis). This result may indicate that more attention should be paid to the difference in the responses of high angiogenesis tumors.

There were several limitations to this study. First, the A549 and PC-3 lines represent different cancer types, and this could easily raise questions regarding the validity of this

experimental scheme with regard to the treatment efficacy in different tumor types from the same type of cancer. These two xenografted tumor-bearing animal models (A549 with relatively high integrin αvβ3 expression in the tumor cells and tumor neovasculature; and PC-3 with low integrin αvβ3 expression in the tumor cells and neovasculature) were verified in previous studies, and it was indeed difficult to find two tumor cell lines of xenografted tumors with significantly different uptakes in RGD PET or SPECT from the same tumor type (28,29). Second, xenografted tumors are relatively homogeneous. The CVs of the tumor uptake in the present study may not be able to completely replace tumor heterogeneity in clinical settings.

In conclusion, in this study, data was obtained supporting the fact that the use of ^{18}F-alfatide PET may be a valid and useful pretreatment screening tool to identify individuals who would benefit from anti-angiogenic drug-containing therapy. The inter- and intra-angiogenic heterogeneity highlighted the importance of individual selection prior to anti-angiogenic therapy. Further clinical evaluations in large cohorts are required to confirm these preliminary findings.

Acknowledgements

The authors specially thank Professor Hongbo Huang (Jiangsu Key Laboratory of Molecular Nuclear Medicine, Jiangsu Institute of Nuclear Medicine, Wuxi, China) for providing assistance with the micro-PET imaging of the mice.

Funding

The present study was partially funded by the Shandong Key Research and Development Plan (grant nos. 2017CXGC1209 and 2017GSF18164), the Outstanding Youth Natural Science Foundation of Shandong Province (grant no. JQ201423), the Jinan Clinical Medicine Science and Technology Innovation Plan (grant no. 201704095), the National Natural Science Foundation of China (grant nos. 81472812 and 81372413) and the National Key Research and Development Program of China (grant no. 2016YFC0904700).

Availability of data and materials

The datasets obtained during the current study are available from the corresponding author on reasonable request.

Authors' contributions

JY and SY conceived the study, and participated in its design. JL participated in the experiments and drafted the manuscript. DW contributed to the sample collection and interpretation of the data. XS performed the statistical analysis. XM and JL performed the nuclear medicine experiments. SY revised the manuscript. All authors read and approved the final manuscript.

Ethics approval and consent to participate

This study was performed with the approval of the Shandong Cancer Hospital and Institute Ethical Committee, and all the experiments were performed according to the National Institutes of Health Guide for the Care and Use of Laboratory Animals (publication no. 85-23, revised 1985).

Patient consent for publication

Not applicable.

Competing interests

The authors declare that they have no competing interests.

References

1. Folkman J: Role of angiogenesis in tumor growth and metastasis. Semin Oncol 29 (6 Suppl 16): S15-S18, 2002.
2. Folkman J: Angiogenesis in cancer, vascular, rheumatoid and other disease. Nat Med 1: 27-31, 1995.
3. Folkman J: Tumor angiogenesis: Therapeutic implications. N Engl J Med 285: 1182-1186, 1971.
4. Ferrara N and Kerbel RS: Angiogenesis as a therapeutic target. Nature 438: 967-974, 2005.
5. Jayson GC, Kerbel R, Ellis LM and Harris AL: Antiangiogenic therapy in oncology: Current status and future directions. Lancet 388: 518-529, 2016.
6. Kang F, Wang Z, Li G, Wang S, Liu D, Zhang M, Zhao M, Yang W and Wang J: Inter-heterogeneity and intra-heterogeneity of $\alpha_v\beta_3$ in non-small cell lung cancer and small cell lung cancer patients as revealed by ^{68}Ga-RGD$_2$ PET imaging. Eur J Nucl Med Mol Imaging 44: 1520-1528, 2017.
7. Niu G and Chen X: Why integrin as a primary target for imaging and therapy. Theranostics 1: 30-47, 2011.
8. Danhier F, Le Breton AL and Préat V: RGD-based strategies to target alpha(v) beta(3) integrin in cancer therapy and diagnosis. Mol Pharm 9: 2961-2973, 2012.
9. Chen H, Gang N, Hua W and Chen X: Clinical application of radiolabeled RGD peptides for PET imaging of integrin αvβ3. Theranostics 6: 78-92, 2016.
10. Gao S, Wu H, Li W, Zhao S, Teng X, Lu H, Hu X, Wang S, Yu J and Yuan S: A pilot study imaging integrin αvβ3 with RGD PET/CT in suspected lung cancer patients. Eur J Nucl Med Mol Imaging 42: 2029-2037, 2015.
11. Massoud TF and Gambhir SS: Molecular imaging in living subjects: Seeing fundamental biological processes in a new light. Genes Dev 17: 545-580, 2003.
12. Wei YC, Gao Y, Zhang J, Fu Z, Zheng J, Liu N, Hu X, Hou W, Yu J and Yuan S: Stereotactic comparison study of ^{18}F-alfatide and ^{18}F-FDG PET imaging in an LLC tumor-bearing C57BL/6 mouse model. Sci Rep 6: 28757, 2016.
13. Zhang H, Liu N, Gao S, Hu X, Zhao W, Tao R, Chen Z, Zheng J, Sun X, Xu L, *et al*: Can a novel ^{18}F-ALF-NOTA-PRGD2 PET/CT predict the treatment sensitivity of concurrent chemoradiotherapy in patients with newly diagnosed glioblastoma? J Nucl Med 57: 524-529, 2016.
14. Luan X, Huang Y, Gao S, Sun X, Wang S, Ma L, Teng X, Lu H, Yu J and Yuan S: ^{18}F-alfatide PET/CT may predict short-term outcome of concurrent chemoradiotherapy in patients with advanced non-small cell lung cancer. Eur J Nucl Med Mol Imaging 43: 2336-2342, 2016.
15. Tian S, Quan H, Xie C, Guo H, Lü F, Xu Y, Li J and Lou L: YN968D1 is a novel and selective inhibitor of vascular endothelial growth factor receptor-2 tyrosine kinase with potent activity in vitro and in vivo. Cancer Sci 102: 1374-1380, 2011.
16. Becker S, Bohn P, Bouyeure-Petit AC, Modzelewski R, Gensanne D, Picquenot JM, Dubray B and Vera P: Bevacizumab enhances efficiency of radiotherapy in a lung adenocarcinoma rodent model: Role of αvβ3 imaging in determining optimal window. Nucl Med Biol 42: 923-930, 2015.
17. Wan W, Guo N, Pan D, Yu C, Weng Y, Luo S, Ding H, Xu Y, Wang L, Lang L, *et al*: First experience of ^{18}F-alfatide in lung cancer patients using a new lyophilized kit for rapid radiofluorination. J Nucl Med 54: 691-698, 2013.
18. Hu M, Xing L, Mu D, Yang W, Yang G, Kong L and Yu J: Hypoxia imaging with 18F-fluoroerythronitroimidazole integrated PET/CT and immunohistochemical studies in non-small cell lung cancer. Clin Nucl Med 38: 591-596, 2013.

19. Ji S, Zheng Y, Shao G, Zhou Y and Liu S: Integrin $\alpha_v\beta_3$-targeted radiotracer ^{99m}Tc-3P-RGD_2 useful for noninvasive monitoring of breast tumor response to antiangiogenic linifanib therapy but not anti-integrin $\alpha v\beta 3$ RGD_2 therapy. Theranostics 3: 816-830, 2013.
20. Iagaru A, Mosci C, Mittra E, Zaharchuk G, Fischbein N, Harsh G, Li G, Nagpal S, Recht L and Gambhir SS: Glioblastoma multiforme recurrence: An exploratory study of ^{18}F $FPPRGD_2$ PET/CT. Radiology 277: 497-506, 2015.
21. Minamimoto R, Karam A, Jamali M, Barkhodari A, Gambhir SS, Dorigo O and Iagaru A: Pilot prospective evaluation of ^{18}F-$FPPRGD_2$ PET/CT in patients with cervical and ovarian cancer. Eur J Nucl Med Mol Imaging 43: 1047-1055, 2016.
22. Tong RT, Boucher Y, Kozin SV, Winkler F, Hicklin DJ and Jain RK: Vascular normalization by vascular endothelial growth factor receptor 2 blockade induces a pressure gradient across the vasculature and improves drug penetration in tumors. Cancer Res 64: 3731-3736, 2004.
23. Jain RK: Determinants of tumor blood flow: A review. Cancer Res 48: 2641-2658, 1988.
24. Kim KJ, Li B, Winer J, Armanini M, Gillett N, Phillips HS and Ferrara N: Inhibition of vascular endothelial growth factor-induced angiogenesis suppresses tumour growth in vivo. Nature 362: 841-844, 1993.
25. Fukumura D and Jain RK: Tumor microvasculature and microenvironment: Targets for anti-angiogenesis and normalization. Microvasc Res 74: 72-84, 2007.
26. Kang F, Wang S, Tian F, Zhao M, Zhang M, Wang Z, Li G, Liu C, Yang W, Li X, *et al*: Comparing the diagnostic potential of ^{68}Ga-Alfatide II and ^{18}F-FDG in differentiating between non-small cell lung cancer and tuberculosis. J Nucl Med 57: 672-677, 2016.
27. Iagaru A, Mosci C, Shen B, Chin FT, Mittra E, Telli ML and Gambhir SS: ^{18}F-$FPPRGD_2$ PET/CT: Pilot phase evaluation of breast cancer patients. Radiology 273: 549-559, 2014.
28. Zhou Y, Kim YS, Lu X and Liu S: Evaluation of ^{99m}Tc-labeled cyclic RGD dimers: Impact of cyclic RGD peptides and ^{99m}Tc chelates on biological properties. Bioconjug Chem 23: 586-595, 2012.
29. Zhou Y, Kim YS, Chakraborty S, Shi J, Gao H and Liu S: ^{99m}Tc-labeled cyclic RGD peptides for noninvasive monitoring of tumor integrin $\alpha_V\beta_3$ expression. Mol Imaging 10: 386-397, 2011.